Tailoring the Electrooptic Response and Improving the Performance of Integrated $LiNbO_3$ Modulators by Domain Engineering

Davide Janner, Michele Belmonte, and Valerio Pruneri

***Abstract*—Domain inversion (DI) is applied to traveling-wave integrated electrooptic (EO) $LiNbO_3$ modulators to achieve predefined EO frequency response and improved performance with respect to standard single-domain (not domain-inverted) counterparts, including lower driving voltages and larger modulation bandwidths. In particular, when an appropriate poling (DI) is performed along the interaction length, two novel configurations are envisaged. 1) An apodised longitudinal poling profile is used in non-velocity-matched (NVM) modulators to achieve a desired EO response, such as amplitude modulation with intrinsic third-order Bessel-type optical filtering for duobinary transmission. 2) Two-section longitudinal poling is used to counteract the detrimental microwave loss effect in VM modulators and to increase the bandwidth to driving voltage ratio, achieving a value up to 50% larger than that of single-domain (unpoled) structure.**

***Index Terms*—Domain-inverted $LiNbO_3$, electrooptic (EO) modulator, integrated optics.**

I. Introduction

WITH THE increasing demand for broadband communication, optical networks play a crucial role as the primary carrier of the data stream. In this context, high-speed optical modulators are essential for optical transmission systems, and external $LiNbO_3$ modulators are still extremely effective [1], in particular, for long haul and metro applications, as it is shown by their recent increasing commercial demand. $LiNbO_3$ with respect to semiconductor-based modulators market share could even become larger if performance, integration, and cost effectiveness further improve.

The basic scheme for an interferometric Mach–Zehnder amplitude modulator in a single-domain crystal produces a frequency response which has a cardinal sine shape and a limited bandwidth inversely proportional to the length [1]. Both these features have drawbacks in the picture of actual needs for broadband modulation because of the restriction of the bandwidth and because the ripples in the electrooptic (EO) response may negatively affect some transmission formats, e.g., duobinary. A great increase in the EO bandwidth can be achieved with velocity-matched (VM) modulators in which the geometry of the modulator and of the electrodes is arranged so that the velocities of the modulating electrical and optical waves are very close [1], [2]. In this case, the limit on the EO bandwidth is set by the microwave loss dependency on modulation frequency: the higher the frequency, the larger the microwave loss and the shorter the effective interaction length (smaller efficiency). A figure of merit relevant for a modulator is the ratio (BW/V_π) between its EO bandwidth (BW) and switching voltage (V_π). In the design, it is also critical to consider the constraint on the modulator length given by the package dimension requirement as well as the tradeoff between BW and V_π (the larger the length, the lower V_π, but the smaller BW).

Domain inversion (DI) in ferroelectrics, such as $LiNbO_3$, produces a sign reversal of the second-order nonlinear optical properties, including the nonlinear optical coefficient and EO coefficient [3]. It has thus been widely exploited in all-optical processes, e.g., quasi-phase-matched second harmonic generation [4], [5], optical parametric oscillation [6], and wavelength-division multiplexing wavelength conversion [7]. So far, its use in EOs, where one of the interacting fields is at low frequency or a microwave, has been mostly limited to quasi-VM (QVM) devices using periodic structures to produce narrow-band modulation at high frequency [8], [9]. More recently, DI has been used to produce large bandwidth and low driving voltage modulation [10]–[12], a desired chirp value for the output EO-modulated optical wave [13], and to realize single-side-band modulators [14]. When DI (also called poling) is used in a periodic fashion, it allows centering the EO frequency response of interest by simply changing the periodicity of the poling. In this case, a QVM condition is reached, and the center of the cardinal sine is shifted from DC of the single-domain (unpoled) modulator to the desired frequency, while its shape remains qualitatively the same. In the attempt of keeping the advantages of periodically poled modulators while broadening the bandwidth, multiperiod structures, which are constituted by a sequence of different periodically poled zones, have been employed with promising results [15]. DI optimization was inspired by previous work on phase reversal electrodes in single-domain structures [16], [17], which are carried out to produce an adjustable QVM, thus allowing selection of the desired maximum phase change at the frequency of interest by tuning the driving voltage [18], [19].

Manuscript received January 15, 2007; revised May 8, 2007. This work was supported by the Spanish Government through a Juan de la Cierva post-doctoral grant.

D. Janner is with the Institute of Photonic Sciences, 08860 Barcelona, Spain (e-mail: davide.janner@icfo.es).

M. Belmonte is with Avanex Corporation Sede Secondaria, San Donato Milanese (MI), 20097 Milan, Italy (e-mail: michele_belmonte@avanex.com).

V. Pruneri is with the Institut de Ciencies Fotoniques, 08860 Barcelona, Spain, and also with the Institució Catalana de Recerca i Estudis Avançats, 08010 Barcelona, Spain (e-mail: valerio.pruneri@icfo.es).

Color versions of one or more of the figures in this paper are available online at http://ieeexplore.ieee.org.

Digital Object Identifier 10.1109/JLT.2007.901454

In this paper, we propose DI configurations to either tailor the EO response to a predefined shape or increase the BW/V_π ratio. We will focus on the use of DI for changing the EO spatial distribution along the interaction length of a traveling-wave modulator. Two types of DI modulators are proposed. 1) An apodised longitudinal poling profile is used in non-VM (NVM) modulators to achieve a desired EO response. 2) Longitudinal poling is used in VM modulators to counteract the effect of microwave loss on bandwidth. In the former case, by using an apodisation technique that is similar to that of fiber Bragg gratings, we demonstrate the possibility to induce a predefined EO frequency response, and as an example, we report the synthesis of a third-order Bessel-type modulation without the need of any additional electrical filter, which is suitable for duobinary transmission [20]. In the latter case, we propose a simple technique for flattening the EO frequency response, which is similar to what is done for wavelength-dependent optical gain in Er-doped fiber amplifier (EDFA). The response is worsened more at lower frequency by inverting the sign of the EO interaction at the modulator end. In this way, we achieve BW/V_π figure of merits which are up to 50% higher than those in single-domain structures. The structure of this paper is as follows: In Section II, we will outline some basic concepts to analyze the novel proposed designs presented in Section III. In Section IV, some conclusions will be drawn.

II. Background

In order to present our results, we summarize the main principles and equations of a traveling-wave z-cut $LiNbO_3$ modulator, with straight electrodes perfectly impedance-matched, 50/50 power splitting [1], [2], and perfect symmetry of the electrical and electrooptical parts between the two arms. In such a modulator, the traveling microwave voltage amplitude along the arms can be written as

$$V(x) = V_0 \sin(k_m \cdot \delta \cdot x - 2\pi f_m t_0) \tag{1}$$

where V_0 is the amplitude of the wave, $k_m = 2\pi n_m/\lambda_m$ is the microwave wavenumber, $\delta = 1 - n_{\text{opt}}/n_m$ is the relative mismatch between the refractive index of the microwave (n_m) and optical (n_{opt}) waves, f_m is the microwave frequency corresponding to the wavenumber k_m, and t_0 accounts for an initial phase mismatch between optical and microwave fields. Driven by the microwave, the phase change experienced by the optical wave at the end of the modulator can be written as

$$\Delta\phi(f_m) = \int_0^L -\frac{2\pi}{\lambda}\frac{n_{\text{opt}}^3}{2} r \frac{\Gamma}{G} \cdot p(x) \cdot V_0 \sin[k_m \cdot \delta \cdot x - 2\pi f_m t_0] dx \tag{2}$$

where L is the length of the arms of the modulator itself, λ is the optical wavelength, r is the EO coefficient (in our case for $LiNbO_3$, $r = r_{33}$), G is the spatial gap between the two electrodes, and Γ is the overlap integral between the optical and microwave electric fields defined as [21]

$$\Gamma = \frac{G}{V_0}\frac{\int\int E_m \cdot |E_o|^2 dS}{\int\int |E_o|^2 dS} \tag{3}$$

with E_m and E_o being the microwave and optical fields, and the integration domain being a plane transversal to the modulator propagation direction. The function $p(x)$ in (2) is the poling profile and accounts for changes in the EO response along the modulator due to $LiNbO_3$ DI. This function may have two discrete values, either $+1$ or -1. For example, for unpoled (not inverted) modulators, the function $p(x) = +1$ and is constant over the entire length. From (2), we may derive the switching voltage (V_π) corresponding to a phase change of π over the interaction length (L) when a theoretical zero optical output occurs, namely

$$V_\pi = \frac{\lambda \cdot G}{2n_{\text{opt}}^3 L \cdot r \cdot \Gamma}. \tag{4}$$

This expression shows the inverse dependence on the length of the modulator. Since it is a critical parameter in real systems because of the limitations on the driver voltage output with increasing frequency, the design of the device should also account for lowering this value.

Besides, in a real modulator, one of the main limitations to the modulation bandwidth is represented by the microwave losses along the electrodes. For this reason, we also include in our analysis these losses which can be computed using a finite-element-method (FEM) program [18]. If we account for the microwave losses, the driving voltage expression may be rewritten as

$$V(x,t) = V_0 \cdot e^{-\alpha(f_m)\cdot x} \cdot e^{j(k_m \cdot \delta \cdot x - 2\pi f_m t_0)}. \tag{5}$$

Now reconsidering (2) and including microwave propagation loss, the EO response for a single-domain (unpoled) modulator, $p(x) = 1$ everywhere, can be defined as the normalized quantity

$$m(f) = \left|\frac{\Delta\phi(f)}{\Delta\phi(0)}\right| = e^{-\frac{\alpha L}{2}} \sqrt{\left[\frac{\sinh^2\left(\frac{\alpha L}{2}\right) + \sin^2\left(\frac{\xi L}{2}\right)}{\left(\frac{\alpha L}{2}\right)^2 + \left(\frac{\xi L}{2}\right)^2}\right]} \tag{6}$$

where $\xi = 2\pi f_m(n_m - n_{\text{opt}})/c_0$, with c_0 being the speed of light in vacuum. If we neglect the losses in (6), we obtain the sinc behavior of the most classical modulator having $m(f) = \text{sinc}(\xi L/2)$, as shown in Fig. 1. In this case, the bandwidth can be estimated as

$$\text{BW} = \frac{1.4 \cdot c}{\pi(n_m - n_{\text{opt}})L} \tag{7}$$

which shows that, in first approximation, BW depends on the inverse of the length of the modulator arm and on the index mismatch between the electrical and optical waves. Considering (4) and (7), we see a tradeoff between a large bandwidth and a

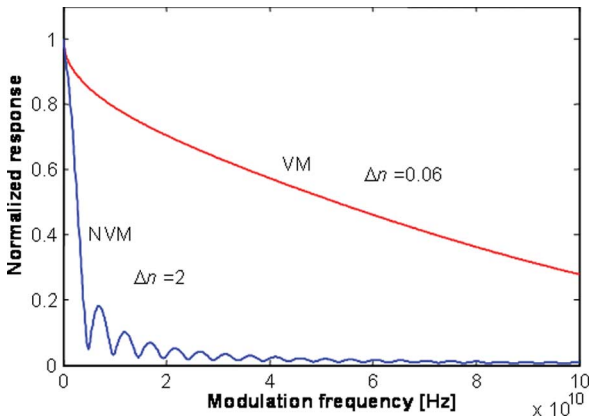

Fig. 1. Comparison between NVM (blue line) and VM modulators (red line). In the case of VM modulator, $\Delta n = 0.06$ is reported to appreciate the difference with NVM modulator. The ideal VM case ($\Delta n = 0$) would produce a constant normalized response of one over an infinite range.

low switching voltage due to their inverse dependence on L. A solution to this problem is represented by the reduction of the index mismatch, which results in an increase of the bandwidth without any change in the switching voltage V_π. For this reason, the solution of VM [1], [18] is the most popular to significantly increase the bandwidth. In Fig. 1, the normalized response for a VM modulator having a small index mismatch ($\Delta n = 0.06$) is reported in order to be compared to the sinc response of an NVM modulator. The response of VM modulators depends much more on the microwave losses than the NVM ones, and the introduction of buffer dielectric layers under the electrodes, to obtain the VM condition, may increase V_π since the coupling between electrical and optical fields [Γ in (4)] is usually lowered.

In order to achieve modulation at higher frequencies without employing VM modulators, QVM via periodic DI engineering may be used. In this case, the poling profile $p(x)$ is periodic, and the EO response has still a sinc behavior, but is centered at a specific frequency directly correlated to the period, as shown in Fig. 2(a). This solution gives the possibility to modulate at high frequency, but it undergoes the same limitations about bandwidth and switching voltage to which it is subjected to the unpoled modulator. Moreover the bandwidth can turn out to be small for some application purposes. In order to broaden the bandwidth in such tailored response modulators, multi-period structures have also been proposed [15]–[17] in which different periodic poling profiles are placed in an appropriate sequence resulting in an overall bandwidth increase, as shown in Fig. 2(b). In this case, the modulator is usually longer, and an increase in the switching voltage is produced. The extension of this concept of domain engineering to completely aperiodic structure in NVM modulators can lead to design precise EO response modulators.

III. Proposed Domain-Inverted Modulator Designs

By applying the EO response tailoring concept through engineering of the different sign EO domains, we propose two innovative structures in NVM and VM configurations, respectively.

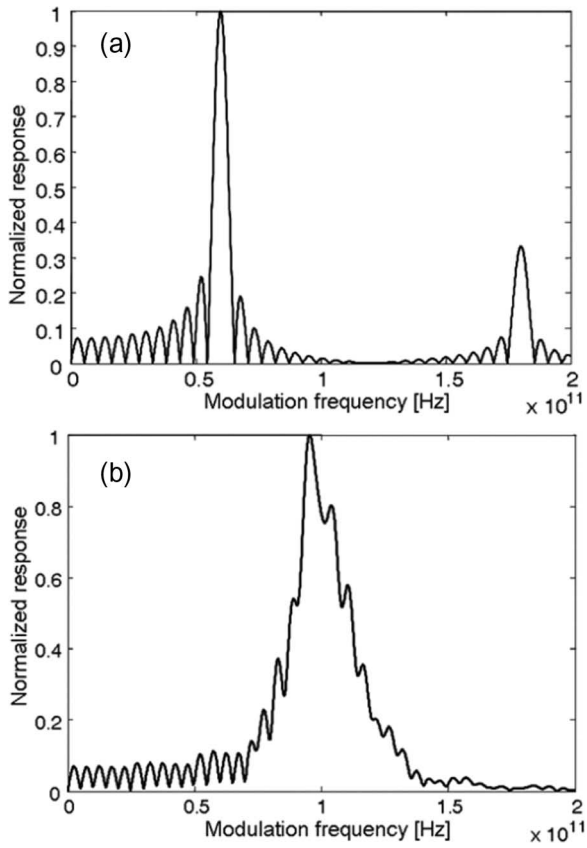

Fig. 2. Normalized EO response of QVM modulators for (a) periodically poled $LiNbO_3$ centered at 6 GHz and (b) multiperiod sequence of periodically poled domains.

A. Precise EO Response Modulator

Let us consider the following identity:

$$P(f) = \int_{-\infty}^{+\infty} p(x) \cdot e^{-j2\pi f x} dx = \int_{-\infty}^{+\infty} p(x) \cdot \cos(2\pi f x) - j \int_{-\infty}^{+\infty} p(x) \cdot \sin(2\pi f x) \quad (8)$$

in which the imaginary part is very similar to (2), provided that we extend the integration domain to infinity and introduce a rectangular window function to account for the finiteness of the poled region. Now, identity 8 allows us to write the phase change in (2) (assuming without loss of generality $t_0 = 0$) in terms of the Fourier transform of the poling function as

$$\Delta\phi'(t_0) = \frac{2\pi}{\lambda} \frac{n_{\text{opt}}^3}{2} r \frac{\Gamma}{G} V_0 \cdot \text{Im}\left\langle F\left[p(x)\right] \cdot e^{j2\pi f t_0} \right\rangle \quad (9)$$

in which the constants have the same meaning as in (2), and the symbol F denotes the Fourier transform of the window $p(x)$ function. Thus, the response of the modulator can be obtained numerically via a simple fast Fourier transform (FFT) of the

poling function, and the relationship between the modulation frequency and the computed frequency of the FFT is given by

$$k_m \cdot \delta = 2\pi f \rightarrow f_m = \frac{c}{N \cdot T \cdot \Delta n} l, \Delta f = \frac{c}{N \cdot T \cdot \Delta n} \tag{10}$$

where N is the number of discrete samples into which the poling function $p(x)$ is divided, T is the width of one sample, l is an integer number ranging from 0 to $N-1$, $\Delta n = n_m - n_{\text{opt}}$ is the index mismatch as previously defined, and Δf is the frequency step. We also note that electrical losses of the modulating wave may be included in the computation by the substitution $p(x) \rightarrow e^{-\alpha x} p(x)$ in (9). Where otherwise not stated, we assume the loss parameter $\alpha(f) = k\sqrt{f}$ with $k = 0.51\ (\text{cm} \cdot \text{GHz})^{-1/2}$, which is a typical value and may be computed by well-known methods [18]. In our case, we obtained the constant k by fitting the experimental results of a typical modulator up to 40 GHz using FEM techniques. The advantage of this formulation of the modulator response as in (9) is that a straightforward inversion could be obtained by the simple relation:

$$h(x) = \text{Re}\left\langle F^{-1}\left[\Delta\phi_0(f)\right]\right\rangle \tag{11}$$

where F^{-1} is the inverse Fourier transform, and $\Delta\phi_0(f)$ is the desired frequency response of the modulator. Thus, we may recover a continuous poling function from a desired frequency response. Also in this case, an FFT algorithm can be employed, and with analogous consideration as in the direct case, the following relationships can be obtained:

$$T = \frac{c}{N \cdot \Delta f \cdot \Delta n} \quad L = NT = \frac{c}{\Delta f \cdot \Delta n} \tag{12}$$

where T is the spatial step into which the poling function $h(x)$ is sampled, N is the number of discrete samples considered, Δf is the step in frequency, Δn is the index mismatch, and L is the total length of the modulator. The function $h(x)$ in (11) is a continuous function assuming different values from -1 to $+1$. Thus, in order to recover the apodised poling profile $p(x)$, which assumes only two discrete values (-1 or $+1$), we must provide an algorithm to quantize the continuous function $h(x)$ analogously to the apodisation technique used in fiber Bragg grating design. Let us divide the $h(x)$ into a large number of sections of length L_s and consider also the target poling function $p(x)$ that is composed by equally spaced subdomains, each of size L_s/N, where $N > 1$ is an integer. If we compute the mean value $\overline{h}_i$ of $h(x)$ on the ith section, the translation of that mean value in terms of the poling function $p(x)$ is obtained by letting the mean value of $p(x)$ on that section coincide with $\overline{h}_i$. For example, if we assume for a single section that $\overline{h}_i = -0.4$, this means that 30% of the subdomains defined by the square wave $p(x)$ in that section must be set to $+1$, and the other 70% of the poling subdomains must be set to -1, so that $0.31 + 0.7 \cdot (-1) = -0.4$. The mean value $\overline{h}_i$ of the continuous function $h(x)$ is easily reported to the poling function $p(x)$ in this way by simply imposing a length $L_p^- = 0.7L_s$ of the section to -1 and a length $L_p^+ = 0.3L_s$ to $+1$.

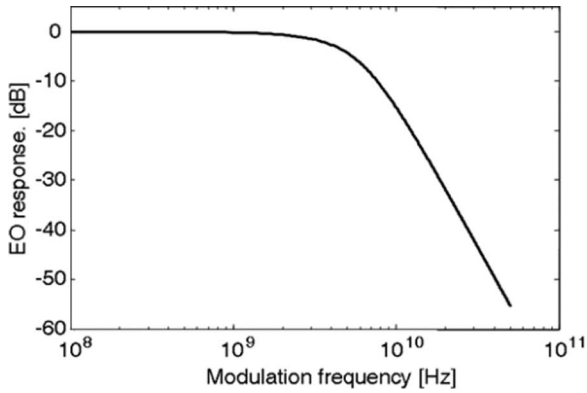

Fig. 3. Desired EO response for a third-order Bessel filtering modulator with a -6-dB cutoff frequency of 6 GHz.

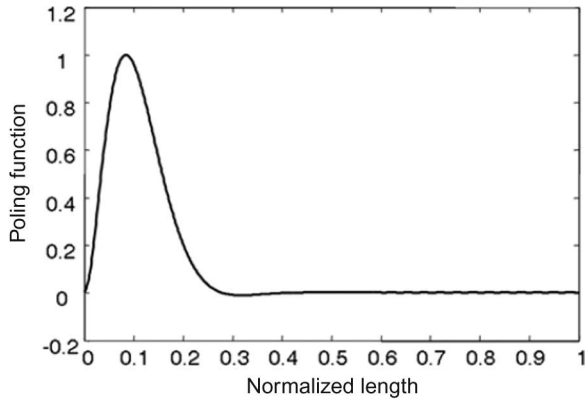

Fig. 4. Reconstructed poling function $h(x)$ which produces the desired Bessel filter response.

This approximation is valid since we assumed that the section length L_s is much smaller compared to the coherence length of the microwave ($\lambda_m/2\Delta n$, about 750 μm at 10 GHz), and the phase modulation in this case has an almost linear response with no sensitivity on the order of the subdomains of $p(x)$ in the single section. The size of the section length L_s, in principle, is arbitrary. Two important features have to be guaranteed: The poling function $h(x)$ needs to be sufficiently smooth [i.e., $h(x)$ variation over L_s is small], and the structure needs to be practically realizable. For example, L_s can be set at 50–70 μm (minimum domain size is in the range of 10 μm), small to appreciate any variation of $h(x)$ over it and still sufficiently large for the DI to be realized with high yield.

To illustrate the potential of this technique, we report here, as an example, a modulator having an EO response of a third-order Bessel filter with a -6-dB cutoff frequency of 6 GHz. This kind of filter is very useful in the duobinary format transmissions, where the tails of the typical cardinal sine response of normal modulators have negative effects, and an electrical filter is usually needed to cut them off [20]. Starting from the desired EO response reported in Fig. 3 and applying the inverse Fourier transform algorithm of (11), we obtain the continuous poling profile $h(x)$, as reported in Fig. 4. The poling function here is plotted against a normalized length $L' = \Delta n \cdot L \cdot \Delta f / c = 1$ since, in this first stage of the design, we neglect the microwave losses and assume that the EO response does not depend on

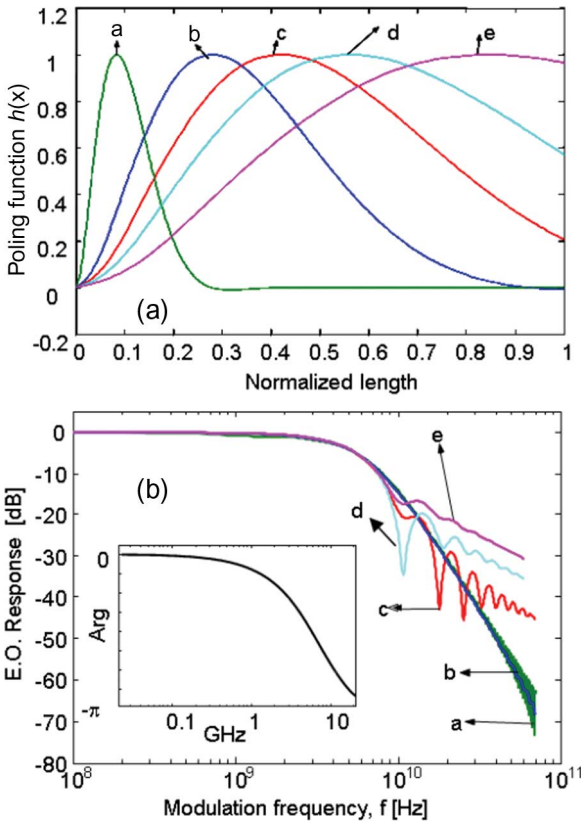

Fig. 5. Comparison of the (a) different poling functions and their (b) EO response for the following: 1) ideal case ($V_\pi = 99$ V $\cdot$ cm) or truncated to 2) the first lobe ($V_\pi = 30$ V $\cdot$ cm); (c) two-third of the first lobe ($V_\pi = 21$ V $\cdot$ cm); (d) one-half of the first lobe ($V_\pi = 18.6$ V $\cdot$ cm); (e) one-third of the first lobe ($V_\pi = 20.1$ V $\cdot$ cm). The inset plots the phase response of the modulator comprising one lobe truncating the poling function as in (b).

the length by keeping the product $\Delta n \cdot L$ constant. In such a way, we can consider the length L and the index mismatch Δn design parameters to be decided a posteriori depending on the EO response and including the microwave losses. By observing the recovered poling function in Fig. 4, we note that the longest part of it is nearly zero, almost not influencing the modulation of the phase. Moreover, the average of the function $h(x)$ over the domain can be used to estimate $V_\pi = 99$ V $\cdot$ cm, which is extremely large. Thus, from these considerations, we can argue that the last part of the poling function, which is nearly zero, could be disregarded in the modulator design and dropped.

To address this point in Fig. 5(a) and (b), we report the comparison of the ideal and some poling functions obtained by truncation of the ideal one and their respective EO responses. We note that the switching voltage is inversely proportional to the area under the poling curve, and moreover, the more truncated the poling function, the worse the EO response (ripples). In Fig. 5(b), we may also note that the closest response to the ideal case of the third-order Bessel filter is the function truncated at the first lobe, which is differentiating its response from the ideal one only by negligible ripples at higher frequencies. Moreover, this profile has a much lower $V_\pi = 30$ V $\cdot$ cm. In the inset of Fig. 5(b), we plot also the phase response of the one-lobe modulator for the sake of completeness.

Once the single-lobe function is chosen as our poling function, we may account for electrical losses. If we compare the

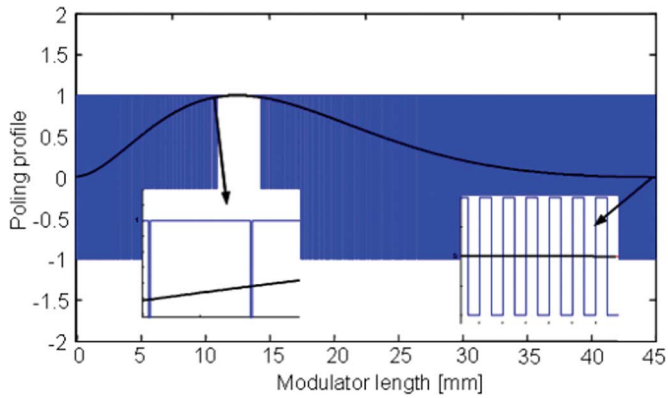

Fig. 6. Continuous poling function (black solid) and reconstructed discrete valued profile function (blue line).

EO responses with and without microwave loss, for a constant $\Delta n \cdot L$, we note that they depend on the device length. Indeed, with respect to the ideal (no microwave loss) EO response, the behavior that accounts for the loss ($\alpha = 0.49\sqrt{f}$ dB/cm) for a modulator of length $L = 45$ mm and $\Delta n = 1.32$ remains qualitatively the same, with the exception of the cutoff frequency that, from the 6-GHz ideal case, is reduced to about 5.25 GHz. However, the 6-GHz bandwidth could be achieved by initially designing the ideal structure (no losses) having a larger cutoff frequency, so that after accounting for microwave loss, the EO response becomes the desired one.

The final apodised poling profile $p(x)$ for the designed Bessel-type modulator with a cutoff frequency at -6 dB of 6 GHz is reported in Fig. 6 and compared with the continuous poling function $h(x)$. Such a modulator has a switching voltage of 6.6 V.

The proposed design is for a modulator that can be used for a 10-Gb/s transmission. The common approach consists of third-order Bessel-type electrical filtering of a standard 10-Gb/s modulator, which results in a typical driving voltage of about 5 V. Note that, in comparison, the driving voltage in our case is slightly higher, but could be reduced by increasing the transverse overlap (Γ) which, in the case of classical modulators, would not be possible because the VM condition imposes severe geometrical constraints.

The DI engineering procedure for precise EO response design is straightforward, requiring only simple numerical operations as an inverse Fourier transform and a small number of empirical tries providing precise results. No particular geometry of the electrodes is required, considering only straight lines, thus avoiding curvatures which cause reflections or the modification of the Γ coefficients, effects that can induce different phase changes in the two branches of the modulator producing residual chirp. Moreover, the possibility of tailoring the desired EO response and integrating optical filtering makes this technique appealing for the design of commercial modulators.

B. Flat Response Wide Bandwidth Modulator

In order to widen the bandwidth of EO modulators, the VM approach is very attractive because of the large bandwidth

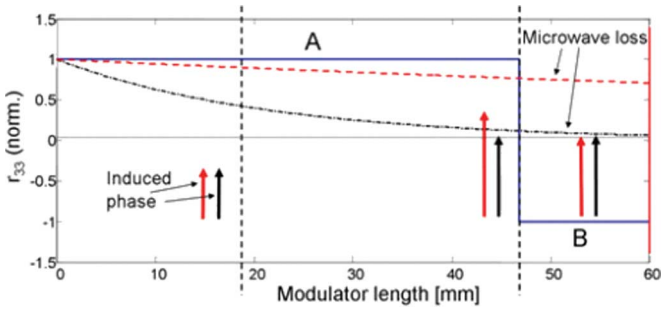

Fig. 7. Schematics of phase change during propagation in a modulator with two sections with (A) normal and (B) inverted EO coefficients. Low frequency response is indicated in red (dashed) and high frequency in black (dash-dotted).

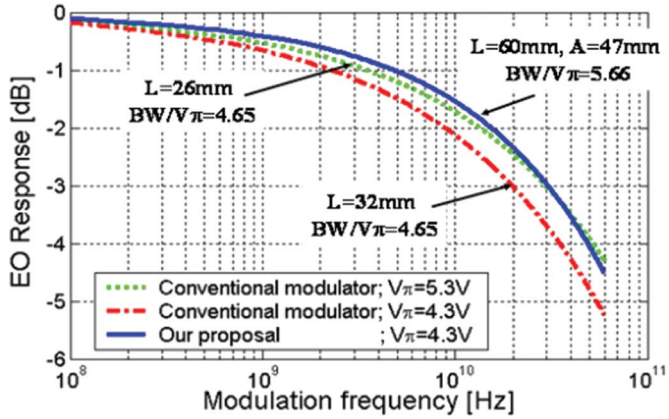

Fig. 8. Comparison of frequency EO response between the proposed modulator (blue) and other two single-domain (unpoled) modulators having the same bandwidth (green) or the same driving voltage (red).

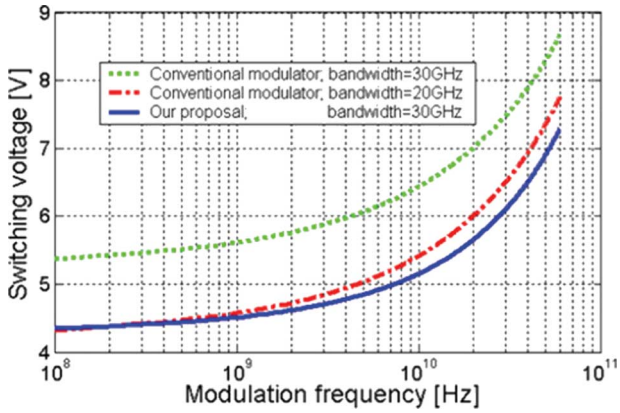

Fig. 9. Switching voltages of the three modulators compared in Fig. 8.

achievable. It is clear that the approach proposed above to tailor the EO response to a predefined shape is not applicable to VM modulators: The periodic or aperiodic DI for such type of modulators has no appreciable results since its real effectiveness is strictly connected to the presence of index mismatch. Indeed, in the VM case, microwave losses become more important than EO spatial distribution in the computation of the EO frequency response (see (2) with $\delta = 0$).

The different attenuation of microwave field with frequency suggests a different DI engineering approach to improve the VM modulator response. The linear response of phase change with length and the fact that higher frequency microwave fields interact with the optical wave over a distance shorter than that of lower frequency fields can be exploited to flatten the response of a VM modulator. Indeed, if we consider a modulator with a first noninverted zone A and a second inverted zone B, as illustrated schematically in Fig. 7, the result of the discontinuity in r (in combination with phase–velocity matching) is that the device operates in three successive zones along the modulator length. In the upstream zone, desirable phase modulation of the optical wave is induced for all microwave frequencies in the bandwidth of the device. In the middle zone, desirable phase modulation is induced for frequencies in the upper part of the bandwidth, but phase modulation in the lower frequencies becomes excessive. At last, in the downstream zone, there is no significant phase modulation at higher frequencies, but the excess modulation at lower frequencies is reduced by the fact that phase modulation has opposite sign with respect to the upstream and middle zones.

In this way, the overall phase change of the modulated optical wave can be equalized by properly choosing the lengths A and B. The obtained flattening in the EO response is conceptually similar to the gain flattening operated in EDFA, in which the higher gain is sacrificed in some zones of the spectrum in order to obtain a flat response.

Now, let us consider the proposed DI geometry for a modulator of length L constituted by two parts of length A and B, respectively $(L = A + B)$, where the first one is not inverted and the second one is inverted. Moreover, let us set the frequency to which the response is flattened to $f_{-3\,\mathrm{dB}}$, which will be the cutoff frequency of our modulator. Now, we can determine the length of the modulator to be inverted by imposing that the total phase change at $f_{-3\,\mathrm{dB}}$ is 3 dB lower than the DC one, namely

$$\begin{aligned}\frac{\sqrt{2}}{2}\cdot K\cdot(A-B)&\\ &= K\int_0^A e^{-\alpha_0 x}\cdot\sin(k_{m,-3\,\mathrm{dB}}\cdot\delta\cdot x - 2\pi f_{-3\,\mathrm{dB}}t)dx\\ &+ -K\int_A^L e^{-\alpha_0 x}\cdot\sin(k_{m,-3\,\mathrm{dB}}\cdot\delta\cdot x - 2\pi f_{-3\,\mathrm{dB}}t)dx\end{aligned} \tag{13}$$

where we considered the DC phase change to be linear, the factor $\sqrt{2}/2$ accounts for the 3-dB lowering with respect to DC, the minus sign multiplying B accounts for the negative phase change, $\alpha_0 = \alpha(f_m = f_{-3\,\mathrm{dB}})$ is the value of the loss at the cutoff frequency, and K indicates the other constants which can be taken out of the integral in (2). Now, (13) can be further simplified by considering a perfect VM $(\delta = 0)$, and it can be rewritten as

$$\frac{\sqrt{2}}{2}\cdot(2A-L) = \frac{1}{\alpha_0}[1-2e^{-\alpha_0 A}-e^{-\alpha_0 L}] \tag{14}$$

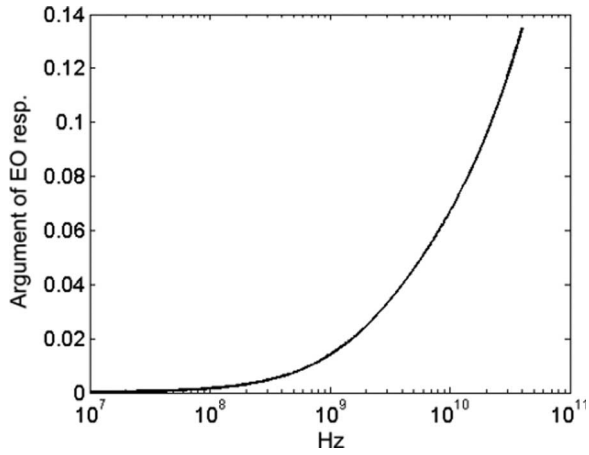

Fig. 10. Phase response for the proposed modulator.

which is a transcendental equation and can be solved numerically with standard techniques. The solution obtained for A will provide an approximate value around which further optimization can be done.

We compare the results of a modulator having a total length of $L = 60$ mm, an index mismatch of $\delta = 0.05$, a bandwidth of 30 GHz, and a switching voltage of $V_\pi = 4.3$ V with the calculated length of $A = 47$ mm with two traditional modulators: one having the same bandwidth and the other having the same switching voltage. As shown in Figs. 8 and 9, the designed modulator has a switching voltage that is 20% lower for equal bandwidth and a bandwidth that is 50% larger for equal voltage. Moreover, the phase response of the modulator has small absolute variation with respect to frequency due to the VM configuration (see Fig. 10).

Thus, in the proposed design, the improvement of BW/V_π figure of merit has been significantly increased at the expense of a longer modulator length, which can be acceptable for those applications not requiring high integration and where performances are more important than the overall length, as for example in aerospace and defense.

IV. Conclusion

We have engineered DI in both NVM and VM integrated EO modulators to demonstrate tailoring of EO response and improvement of BW/V_π figure of merit. In the NVM case, we have demonstrated the possibility to obtain a precise EO frequency response using an apodised DI and corresponding EO coefficient distributions. This technique has allowed the design of a modulator with third-order Bessel-type filtering, which is integrated at optical level, making it useful for duobinary transmitters without the need of any additional electronic components. In the VM case, we have used DI to counteract EO bandwidth limits associated to microwave propagation loss. In fact, we have obtained the flattening of the EO frequency response by making a simple DI, which, in turn, reduces EO efficiency more at low than at high frequencies. However, if we let the interaction length to increase, BW/V_π can be larger (up to 50%) than that achievable in single-domain (unpoled) modulators.

References

[1] E. L. Wooten, K. M. Kissa *et al.*, "A review of lithium niobate modulators for fiber-optic communications systems," *IEEE J. Sel. Topics Quantum Electron.*, vol. 6, no. 1, pp. 69–81, Feb. 2000.

[2] K. W. Hui, K. S. Chiang *et al.*, "Electrode optimization for high-speed traveling-wave integrated optic modulators," *J. Lightw. Technol.*, vol. 16, no. 2, pp. 232–238, Feb. 1998.

[3] R. S. Weiss and T. K. Gaylord, "Lithium niobate: Summary of physical properties and crystal structure," *Appl. Phys. A, Solids Surf.*, vol. 37, no. 4, pp. 191–203, 1985.

[4] M. Yamada, N. Nada, M. Saitoh, and K. Watanabe, "First-order quasi-phase-matched $LiNbO_3$ waveguide periodically poled by applying an external electric field for efficient blue second harmonic generation," *Appl. Phys. Lett.*, vol. 62, no. 5, pp. 435–436, Feb. 1, 1993.

[5] V. Pruneri, R. Koch, P. G. Kazansky, P. S. J. Russell, and D. C. Hanna, "49 mW of cw blue light generated by first-order quasi-phase-matched frequency doubling of a diode-pumped 946 nm Nd:YAG laser," *Opt. Lett.*, vol. 20, no. 23, pp. 2375–2377, Dec. 1995.

[6] L. E. Myers, R. C. Eckardt, M. M. Fejer, R. L. Byer, W. R. Bosenberg, and J. W. Pierce, "Quasi-phase-matched optical parametric oscillators in bulk periodically poled $LiNbO_3$," *J. Opt. Soc. Amer. B, Opt. Phys.*, vol. 12, no. 11, pp. 2102–2116, Nov. 1995.

[7] G. Schreiber, H. Suche, Y. L. Lee, W. Grundkötter, V. Quiring, R. Ricken, and W. Sohler, "Efficient cascading difference frequency conversion in periodically poled Ti:$LiNbO_3$ waveguide using pulse and cw pumping," *Appl. Phys. B, Photophys. Laser Chem.*, vol. 73, no. 5/6, pp. 501–504, Oct. 2001.

[8] J. H. Schaffner, "Periodic domain reversal electro-optic modulator," U.S. Patent 5 278 924, Jan. 11, 1994.

[9] Y. Lu, M. Xiao, and G. J. Salamo, "Wide-bandwidth high-frequency electro-optic modulator based on periodically poled $LiNbO_3$," *Appl. Phys. Lett.*, vol. 78, no. 8, pp. 1035–1037, Feb. 19, 2001.

[10] V. Pruneri and A. Nespola, "Coplanar integrated optical waveguide electro-optical modulator," U.S. Patent 6 760 493, Jul. 6, 2004.

[11] S. Oikawa, F. Yamamoto *et al.*, "Zero-chirp broadband z-cut Ti:$LiNbO_3$ optical modulator using polarization reversal and branch electrode," *J. Lightw. Technol.*, vol. 23, no. 9, pp. 2756–2760, Sep. 2005.

[12] F. Lucchi, M. Belmonte, S. Balsamo, M. Villa, L. Trevisan, S. Pensa, G. Consonni, C. Emanuele, P. Vergani, M. Sottocorno, and V. Pruneri, "10 Gb/s domain engineered $LiNbO_3$ integrated electro-optic modulator for inexpensive low voltage drivers," presented at the Optical Fiber Commun., Anaheim, CA, 2007, Paper OWH3.

[13] N. Courjal, H. Porte, J. Hauden, P. Mollier, and N. Grossard, "Modeling and optimization of low chirp $LiNbO_3$ Mach–Zehnder modulators with an inverted ferroelectric domain section," *J. Lightw. Technol.*, vol. 22, no. 5, pp. 1338–1343, May 2004.

[14] H. Murata and Y. Okamura, "Guided-wave optical wavelength-manipulating devices using electrooptic effect," in *Photonics Based on Wavelength Integration and Manipulation*. Tokyo, Japan: IPAP, 2005, pp. 213–224.

[15] X. F. Chen, X. L. Zeng, Y. P. Chen, Y. X. Xia, and Y. L. Chen, "Optimal design of broadened flat bandpass electro-optic phase modulator based on aperiodic domain-inverted grating," *J. Opt. A, Pure Appl. Opt.*, vol. 5, no. 3, pp. 159–162, May 2003.

[16] D. Erasme and M. G. F. Wilson, "Analysis and optimization of integrated-optic travelling-wave modulators using periodic and nonperiodic phase reversals," *Opt. Quantum Electron.*, vol. 18, no. 3, pp. 203–211, May 1986.

[17] O. V. Kolokoltsev, C. S. Pérez, and R. A. Correa, "Phase-reversal broadband traveling-wave $LiNbO_3$ electrooptic modulator optimized for time-domain applications by a genetic algorithm," *IEEE J. Quantum Electron.*, vol. 8, no. 6, pp. 1258–1264, Nov./Dec. 2002.

[18] S. Haxha, B. M. A. Rahman, and R. J. Langley, "Broadband and low-driving-power $LiNbO_3$ electrooptic modulators," *Opt. Quantum Electron.*, vol. 36, no. 14, pp. 1205–1220, Nov. 2004.

[19] L. N. Binh, "Lithium niobate optical modulators: Devices and applications," *J. Cryst. Growth*, vol. 288, no. 1, pp. 180–187, Feb. 2006.

[20] P. Bravetti, L. Moller, G. Ghislotti, C. Cavalli, C. Gualandi, and P. Bergamini, "Impact of response flatness on duobinary transmission performance: An optimized transmitter with improved sensitivity," *IEEE Photon. Technol. Lett.*, vol. 16, no. 9, pp. 2159–2161, Sep. 2004.

[21] R. C. Alferness, "Waveguide electrooptic modulators," *IEEE Trans. Microw. Theory Tech.*, vol. MTT-30, no. 8, pp. 1121–1137, Aug. 1982.

Davide Janner received the "Laurea" in physics from the Università degli Studi di Milano, Milan, Italy, in 2002, and the Ph.D. degree in physics from the Politecnico di Milano, Milan, in 2006.

He is currently a Postdoctoral Researcher with the Institute of Photonic Sciences, Barcelona, Spain, carrying out research in micro- and nanostructured integrated electrooptic modulators in ferroelectrics. His previous research interests include superluminal propagation of electrons, fiber Bragg gratings, photonic crystals, and slow light propagation.

Michele Belmonte received the Laurea degree (cum laude) in nuclear engineering from the Polytechnic Institute of Milan, Milan, Italy, in 1998.

He joined Pirelli Componenti Ottici, Italy, in May 1999 (acquired by Corning Inc. in 2000 and then by Avanex Corporation Sede Secondaria, in 2003). At Avanex, he is responsible for the system testing of $LiNbO_3$ modulators and management of tunable laser development. Until 2002, he was responsible for fiber Bragg gratings design within the "FBG" activity. He supervised the design of gratings for several applications: dispersion compensation, channel filtering (100- and 50-GHz spacing), Er-doped fiber amplifier gain flattening and pump laser stabilization. He also carried out experimental research on periodic domain inversion of $LiNbO_3$ for frequency conversion and time-resolved spectroscopy. He holds four patents in integrated optic technology, and he has published about 25 papers.

Valerio Pruneri received the Laurea degree in nuclear engineering from Politecnico di Milano (IT), Milan, Italy, and the Ph.D. degree in laser physics/optoelectronics from the University of Southampton, Southampton, U.K.

He is currently a Professor with Institució Catalana de Recerca i Estudis Avançats, Barcelona, Spain, and a Group Leader with the Institut de Ciencies Fotoniques (ICFO), Barcelona. His current applied research interests include micro- and nanoengineered domain-inverted electrooptic devices, phononic/photonic crystals for efficient acoustooptics and microstructured glass fibers (tapered photonic crystal fiber and nanowires) for optical telecommunication, sensing, aerospace, and quantum cryptography. Prior to joining ICFO, he had worked for Avanex Corporation (Italian branch), an optical telecommunication components company based in Milan, which had been previously part of U.S. Corning Inc. and of Pirelli Cables and Systems S.p.A., Italy, from 2000 to 2006, and for the Optoelectronics Research Centre, University of Southampton, from 1993 to 2000. He has received more than 25 invitations at major international conferences. He has authored or coauthored of more than 140 papers, with 14 granted patents/patent applications.

Dr. Pruneri was a recipient of the Philip Morris Prize for scientific and technological research, and he had been a Pirelli Research fellow for several years. He has served on numerous international committees, including the European Conference on Integrated Optics Steering Committee since 2003.